One-neutron halo structure in ^{15}C

D. Q. Fang,[1,2] T. Yamaguchi,[1] T. Zheng,[1,3] A. Ozawa,[1] M. Chiba,[1,4] R. Kanungo,[1] T. Kato,[1] K. Morimoto,[1] T. Ohnishi,[1] T. Suda,[1] Y. Yamaguchi,[1,5] A. Yoshida,[1] K. Yoshida,[1] and I. Tanihata[1]

[1]*The Institute of Physical and Chemical Research (RIKEN), Wako, Saitama 351-0198, Japan*

[2]*Shanghai Institute of Nuclear Research, Chinese Academy of Sciences, Shanghai 201800, China*

[3]*Department of Technical Physics, Peking University, Beijing 100871, China*

[4]*Department of Physics, Tohoku University, Miyagi 980-8578, Japan*

[5]*Department of Physics, Niigata University, Niigata 950-2181, Japan*

(Received 2 January 2004; published 25 March 2004)

The one- or two-neutron removal reactions as well as reaction cross sections for ^{14,15}C on carbon target have been studied by using 110*A* MeV ^{22}Ne primary beam on Riken Projectile Fragment Separator in RIKEN. The longitudinal momentum distributions of ^{13,14}C fragments from ^{15}C and ^{13}C fragments from ^{14}C breakup have been measured at 83*A* MeV by means of direct time-of-flight method. Full width at half maximum (FWHM) of the distributions have been determined to be 71 ± 9 MeV/c and 223 ± 28 MeV/c for ^{14}C and ^{13}C from ^{15}C, and 195 ± 21 MeV/c for ^{13}C from ^{14}C. The FWHM for ^{13}C fragments from ^{15}C and ^{14}C breakup are consistent with the Goldhaber model's prediction. While the FWHM of ^{14}C fragments from ^{15}C is much smaller, which confirms the experimental results from MSU and GANIL, an anomalous enhancement from its neighbors has been observed in the measured reaction cross section of ^{15}C. The experimental data are discussed in the framework of the Glauber model. The analysis of both the fragment momentum distributions and reaction cross sections indicates a dominant *s*-wave component in the ground state of ^{15}C.

DOI: 10.1103/PhysRevC.69.034613 PACS number(s): 25.60.Dz, 25.60.Gc

I. INTRODUCTION

Since the pioneering work with radioactive ion beams (RIBs) at LBL [1], halo structure has become a well-established phenomenon. With the development of accelerator technique for RIBs, numerous experimental as well as theoretical studies have been devoted to nuclei far from the β-stability line regarding the existence of new possible halo nuclei. Experimental methods such as measurement of the reaction cross section (σ_R) and fragment momentum distribution have been widely used to investigate the halo structure. Combined with theoretical analysis, the information about valence nucleon distribution and the nuclear sizes can be extracted from these measured quantities.

^{15}C is a one-neutron halo candidate with small separation energy, $S_n=1.218$ MeV [2], and ground state spin parity $I^\pi=1/2^+$. In measurements of ^{14}C$(d,p)^{15}$C reaction, the reported *s*-wave spectroscopic factors of ^{15}C ground state are 0.99 [3], 0.88 [4], and 1.03 and 0.76 [5], depending on the choice of the distorted-wave Born approximation parameter sets. The momentum distributions of ^{14}C fragment from the breakup of ^{15}C have been measured at MSU and GANIL [6–8]. The extracted widths are much narrower than the Goldhaber model's prediction [9]. It is an indication of a spatially extended matter distribution. Coulomb breakup measurement was reported recently [10]. All these experimental results confirmed the dominant *s*-wave component in the ground state of ^{15}C. On the other hand, the situation in reaction cross section measurement is not so clear. The interaction cross section at relativistic energy showed no peculiarity compared with its neighbor isotopes [11]. While σ_R measurements at intermediate energies more or less exhibited enhancement [12–15]. But it is very interesting that the charge-changing cross section for ^{15}C at relativistic energy was larger than that of ^{14,16}C [16]. For the configuration of valance nucleon, discrepancy has been found in the *s*-wave spectroscopic factor of ^{16}C extracted from the measured fragment momentum distributions and reaction cross sections [17–19]. Similar discrepancy was also found for ^{15}C. From analysis of interaction cross section at relativistic energy the *s*-wave spectroscopic factor resulted in 0.49 ± 0.22 [20], which is much smaller than the values mentioned above. The inconsistent experimental results attracted our attention on this isotope. It is well known that narrow fragment momentum distribution reflects large space distribution of the valence nucleon. Since the effect of the tail in nuclear density distribution is more sensitive at low energy than at high energy, measurements of the fragment momentum distribution and reaction cross section at intermediate energy simultaneously will be very interesting and helpful for understanding of the possible halo structure in ^{15}C.

In this paper we present experimental measurements of the fragment momentum distribution and reaction cross section for ^{14,15}C.

II. EXPERIMENT

The experiment was performed at the Riken Projectile fragment Separator (RIPS) in the RIKEN Ring Cyclotron Facility. The primary beam of 110*A* MeV ^{22}Ne was used to bombard on a Be target (2 mm thick) to produce the secondary beams of ^{14,15}C through projectile fragmentation reaction. Magnetic selection, energy-loss analysis, and time-of-flight (TOF) method were combined to separate and identify the secondary beams. The experimental setup is shown in Fig. 1.

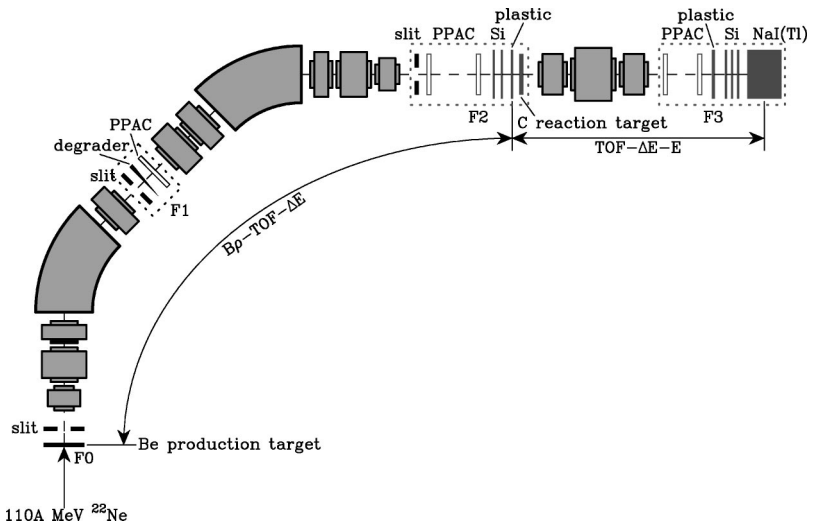

FIG. 1. Experimental setup at the fragment separator RIPS.

At the first dispersive focus in RIPS (F1), an Al wedge-shaped degrader (central thickness, 1098 mg/cm^2; angle, 6 mrad) was used to separate particles by energy-loss method. A delay-line readout Parallel Plate Avalanche Counter (PPAC) was placed to measure momentum broadening of the beam which was confined to ±0.4% by a momentum slit. After passing through F1, the secondary beam was focused onto the achromatic focus F2. Two charge-division readout PPACs were installed to determine the beam position and angle. Two silicon detectors (each 150 μm thick) were used to measure the energy loss (ΔE), and an ultrafast plastic scintillator (0.5 mm thick) was placed before a carbon reaction target (2 mm thick) to measure the TOF from F1-PPAC. The particle identification before the reaction target was done by means of $B\rho$-ΔE-TOF method. The background contamination was estimated to be less than 10^{-4} in the off-line analysis.

After the reaction target, a quadrupole triplet was used to transport and focus the beam onto F3 ($\sim$6 m from F2). The particles were identified by TOF-ΔE-E method. Two delay-line readout PPACs were used to monitor the beam size and emittance angle. Another plastic scintillator (1.5 mm thick) gave a stop signal of the TOF from F2 to F3. To eliminate the channeling effect, three silicon detectors (each 150 μm thick) were used to measure the energy loss (ΔE). The total energy (E) was measured by a NaI(Tl) detector (ϕ3 in. $\times$6 cm, energy resolution of 0.7% in FWHM for 110A MeV ^{22}Ne). The present TOF-ΔE-E method gave us very good charge and mass separation. The particle identification at F3 for Z=6 isotopes is shown in Fig. 2. This spectrum was obtained after gating away fragments with different charge by TOF and ΔE method. The ^{14}C and ^{13}C fragments are well separated from the main peak ^{15}C.

III. FRAGMENT LONGITUDINAL MOMENTUM DISTRIBUTION

A. Experimental results

The longitudinal momentum distributions of fragment from breakup reactions were determined from the TOF between the two plastic scintillators installed at F2 and F3. The position information from F1-PPAC was used to derive the incident momentum. The reaction of the main beam in NaI(Tl) contributed the main background as we could see in Fig. 2. This background was carefully estimated by scaling down the main peak. Then the momentum of fragment relative to the incident projectile in the laboratory frame was transformed into that in the projectile rest frame using the Lorentz transformation. The detailed description of the method can be found in Refs. [18,21]. Under the assumption of a sudden valence-neutron removal, the fragment momentum distribution can be used to describe that of the valence neutron which carries significant information about the structure of nuclei.

Since the magnetic fields of the quadruples between F2 and F3 were optimized for the main beam for the measurement of reaction cross section at the same time. The acceptance for the fragments was simulated by the code MOCADI [18,22]. After correction of transmission effects, the width of momentum distribution is in good agreement with that without correction. Our analysis indicates that transmission correction has very small effect on the momentum distribution.

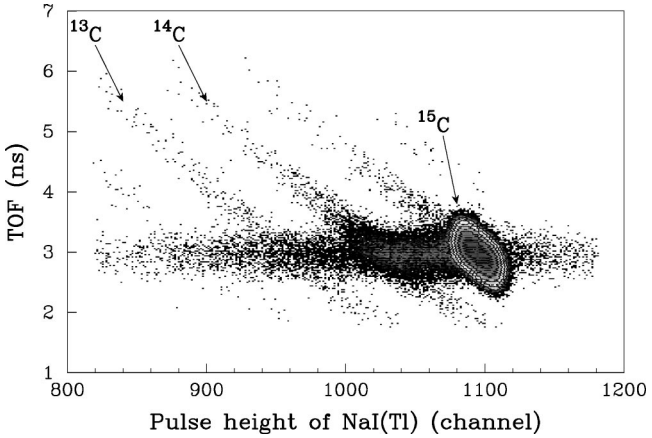

FIG. 2. Particle identification plot at F3 for Z=6 isotopes by using TOF from F2 to F3 and pulse height information from NaI(Tl).

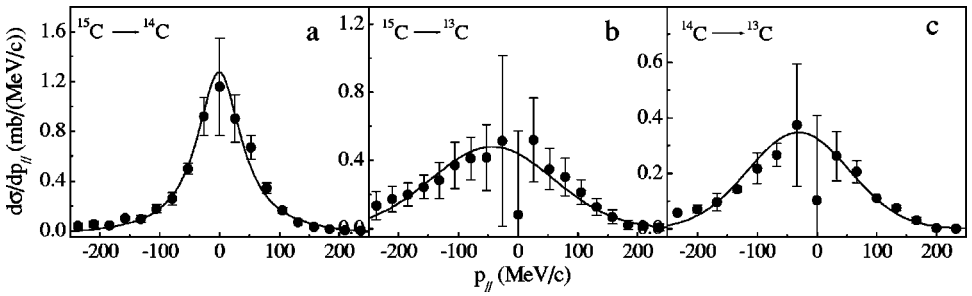

FIG. 3. Fragment longitudinal momentum distributions for ^{15}C $\rightarrow$ ^{14}C (a) ^{15}C $\rightarrow$ ^{13}C (b), and ^{14}C $\rightarrow$ ^{13}C (c) breakup sequences at 83*A* MeV. The dots are experimental data while the lines are fitted results by Lorentzian (a) and Gaussian (b), (c) functions.

The momentum distributions of ^{13,14}C fragments from ^{15}C and ^{13}C fragments from ^{14}C at 83*A* MeV are shown in Fig. 3. In obtaining the momentum distributions, we normalized the experimental counts $[N(p_i)]$ to the measured one- or two-neutron removal cross section (σ_{-1n} or σ_{-2n}) so that $\Sigma N(p_i)\Delta p_{\|}$ equals σ_{-1n} or σ_{-2n}. The error bars in the figure include statistical error as well as error arising from background subtraction. A Lorentzian function was used to fit $^{15}\mathrm{C}\rightarrow{}^{14}\mathrm{C}$ distributions. A Gaussian function was used to fit $^{15}\mathrm{C}\rightarrow{}^{13}\mathrm{C}$ and $^{14}\mathrm{C}\rightarrow{}^{13}\mathrm{C}$ distributions. The FWHMs were determined to be 71 ± 9 MeV/c [Fig. 3(a)], 223 ± 28 MeV/c [Fig. 3(b)] and 195 ± 21 MeV/c [Fig. 3(c)] after unfolding the Gaussian-shaped system resolution ($\sim$20 MeV/c). For $^{15}\mathrm{C}\rightarrow{}^{14}\mathrm{C}$, our result is in agreement with previous experiments which gave 67 ± 3 MeV/c [6] and 64 ± 1 MeV/c [8]. The FWHM for $^{15}\mathrm{C}\rightarrow{}^{13}\mathrm{C}$ is close to the Goldhaber Model's prediction (FWHM=289 MeV/c with σ_0=90 MeV/c) [9]. The FWHM for $^{14}\mathrm{C}\rightarrow{}^{13}\mathrm{C}$ from the present measurement is consistent with the previous value 180 ± 5 MeV/c [8] as well as the Goldhaber Model's prediction (FWHM=212 MeV/c with σ_0=90 MeV/c) [9]. It indicates the bound structure in this nucleus and can be viewed as a check of our experimental method.

Using the estimated transmission value, the one- and two-neutron removal cross sections for ^{15}C were obtained to be 146 ± 23 mb and 177^{+93}_{-49} mb. The σ_{-1n} for ^{14}C was determined to be 67 ± 14 mb. The errors from acceptance estimation were included besides the statistical one. The σ_{-1n} for ^{15}C and ^{14}C are consistent with the results from Ref. [8].

B. Analysis and discussion

There are various theoretical treatments of one-neutron removal process [23–25]. To interpret the measured momentum distributions, we performed a few body Glauber model analysis for $^{15}\mathrm{C}\rightarrow{}^{14}\mathrm{C}$ and $^{14}\mathrm{C}\rightarrow{}^{13}\mathrm{C}$ processes. We assumed a core plus neutron structure for ^{15}C and ^{14}C. The density distribution of the core was supposed to be HO-type function in which the size parameter was adjusted to reproduce the interaction cross section at relativistic energies [20]. The wave function of the valence neutron was calculated by solving the eigenvalue problem in a Woods-Saxon potential. The separation energy of the last neutron was reproduced by adjusting the potential depth. In the calculation the diffuseness and radii parameters were chosen to be 0.67 fm and 1.27 fm. The procedure has been given in Refs. [18,21,26].

We compare the Glauber calculations with the experimental data in Fig. 4. In the figure, the calculated momentum distributions were folded by the Gaussian-shaped experimental system resolution. The considered breakup sequences are shown in the inset of the figure. For the core in excited states, the excitation energy was added to the separation energy of the valence neutron. For ^{14}C, the widths of distributions from breakup to the ground and excited states of ^{13}C are almost same. The calculated distributions can reproduce the experiment data well as shown in Fig. 4(b). For ^{15}C, the breakup to the ground state (0^+) and three excited states (1^-, 0^-, and 2^+) of ^{14}C were calculated. The valence neutrons are in *s*, *p*, *p*, and *d* orbits, respectively. The FWHMs of the calculated momentum distribution for 0^+, 1^-, 0^-, and 2^+ states are 54 MeV/c, 171 MeV/c, 175 MeV/c, and 293 MeV/c respectively. These values are very close to the results from the calculations in the eikonal approximation [25]. In Fig. 4(a), we plot the pure *s*, *p*, and *d* wave components from different sequences with their peaks normalized to the peak of the experimental data. Although the width of the *s* wave is close to the experiment results, none of the calculated distributions can reproduce the data. Then contributions from different sequences were considered. It is assumed that the partial cross section to populate a given final state of the core can be written [27] as

$$\sigma(I_c^{\pi}) = \sum_{nlj} C^2S(I_c^{\pi}, nlj)\sigma_{sp}(nlj), \tag{1}$$

where C^2S is the spectroscopic factor for removed neutron with respect to the core state. σ_{sp} is the single-particle re-

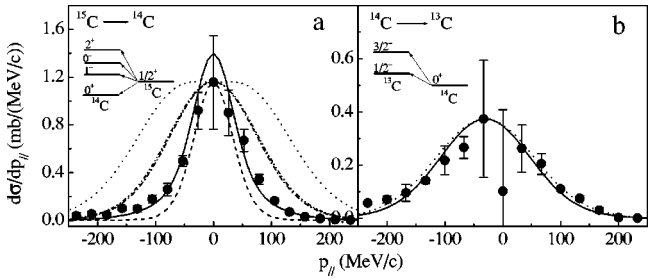

FIG. 4. Fragment longitudinal momentum distributions for ^{15}C $\rightarrow$ ^{14}C (a) and $^{14}\mathrm{C}\rightarrow{}^{13}\mathrm{C}$ (b). (a) The solid line show the best-fit curve obtained by the Glauber analysis based on a core +*n* model. The dashed, dash-doted, dash-dot-doted, and dotted lines show the calculated pure *s*, *p*, *p*, and *d* wave distributions from breakup to the ground state (0^+) and three excited states (1^-, 0^-, and 2^+) of ^{14}C, respectively, with their peaks normalized to the peak of the experimental data. (b) The solid and dotted lines show the *p* wave distribution from breakup to the ground state ($1/2^-$) and excited state ($3/2^-$) of ^{13}C. The insets show the breakup sequences considered in the calculations.

moval cross section. The total inclusive one-neutron removal cross section (σ_{-1n}) is the sum over the cross sections to all core states. In the same way, the momentum distributions from different core state weighted by the corresponding cross section are summed up to get the inclusive momentum distribution.

In order to extract information about the contribution from different breakup sequences, we assumed all the spectroscopic factors as free parameters and adjusted them to fit the momentum distribution of $^{15}C \rightarrow {}^{14}C$. For simplicity, we fixed the ratio between the *s* and *p* wave components using the calculated spectroscopic factors taken from Ref. [8]. Thus $C^2S(1^-)$ and $C^2S(0^-)$ can be calculated from $C^2S(0^+)$ with $C^2S(0^+)$ and $C^2S(2^+)$ being free parameters in our fitting. The solid line in Fig. 4(a) shows the fitted results. From our analysis, contributions of the *s* and *d* wave components to the one-neutron removal cross section are $66\pm13\%$ and $4^{+10}_{-4}\%$, respectively. In a previous experiment, the partial cross sections to different core states were obtained, respectively, by measuring the γ-ray spectra. The experimental contribution of the *d* wave to the removal cross section was only 2% [7]. It was negligible in Coulomb breakup experiment [10]. Our analysis also suggests that contribution from 1 $d_{5/2}$ orbit in the ground state of ^{15}C is very small.

IV. REACTION CROSS SECTION

A. Experimental results

The measurement of reaction cross section was performed with and without a reaction target by a transmission-type method. The reaction cross section was determined by relating the incident and outgoing particles without reaction from both target-in and target-out measurements:

$$\sigma_R = -\frac{1}{t}\ln\left(\frac{\gamma_i}{\gamma_o}\right), \tag{2}$$

where t is the thickness (atom/cm^2) of the reaction target and $\gamma_i(\gamma_o)$ denotes the ratio between outgoing and incident particles with target (without target). In this experiment, the reaction target was carbon with 375 mg/cm^2 thickness. The uncertainty in thickness was less than 0.1%. In determining the reaction cross section, the inelastic reaction was not negligible. The estimated inelastic counts were excluded from the unreacted outgoing events. Since the inelastic events were around 1% ($\sim$25 mb, central value) of the total reaction events, its uncertainty had very small effect on the error of σ_R. Detailed description of the method can be found in Ref. [17].

The determined reaction cross sections for $^{14,15}C$ are given in Table I. The energies refer to the energy in the middle of the reaction target. The errors include statistical one and error from the background and target thickness. The isotopic dependences of σ_R for carbon isotopes measured at low and relativistic energies are compared in Fig. 5. A clear feature is immediately seen in the figure. Strong increase from its neighbors exhibits in σ_R measured at 83*A* MeV for ^{15}C while the experimental data at high energies show almost no effect [20]. It is indicative of anomalous structure in this nucleus.

TABLE I. The reaction cross sections for C isotopes with carbon target measured at RIPS.

Nuclei	Energy (*A* MeV)	σ_R(mb)	Reference
^{12}C	83	957±39	[17]
^{14}C	83	1075±61	Present measurement
^{15}C	83	1319±40	Present measurement
^{15}C	51	1560±44	Present measurement
^{16}C	83	1237±25	[17]

B. Analysis and discussion

In theoretical investigation of reaction cross section, the optical limit Glauber model is widely used. From comparison with experimental data, a systematic underestimation of reaction cross sections at intermediate energies by the optical limit Glauber model was found [28]. A difference factor was defined to describe this underestimation. It was demonstrated that the difference factor was quite different for stable nuclei and nuclei with anomalous structure. Thus it can be used as a criterion to distinguish nuclei with halo structure. To correct the underestimation in the Glauber model, different method has been proposed. A phenomenological correction factor with energy dependence was used in the Glauber model by fitting the ratios of experimental σ_R at low energies to the Glauber calculation [29]. The finite-range effect of nucleon-nucleon collisions was introduced into the Glauber model [17]. The finite-range parameter was determined by fitting the σ_R of $^{12}C+{}^{12}C$ from low energy to relativistic energy.

Using the finite-range Glauber model, the energy dependence of σ_R for ^{14}C was studied. At first the HO-type density distributions were used to reproduce the interaction cross section at relativistic energy, and then the σ_R was calculated by using the fitted size parameter. Underestimation was found at low energies as shown in Fig. 6. The fragment momentum distribution reflects the density distribution of the last nucleon. It was demonstrated that the *p* wave valence

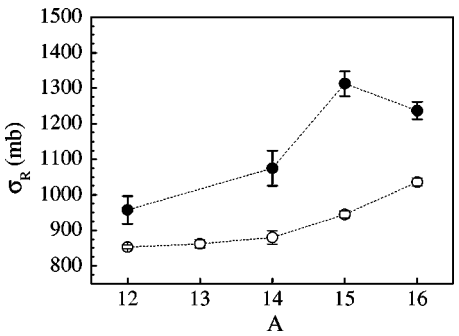

FIG. 5. Isotopic dependence of reaction cross section for C isotopes. The solid and open circles are data measured at 83*A* MeV and relativistic energies [20].

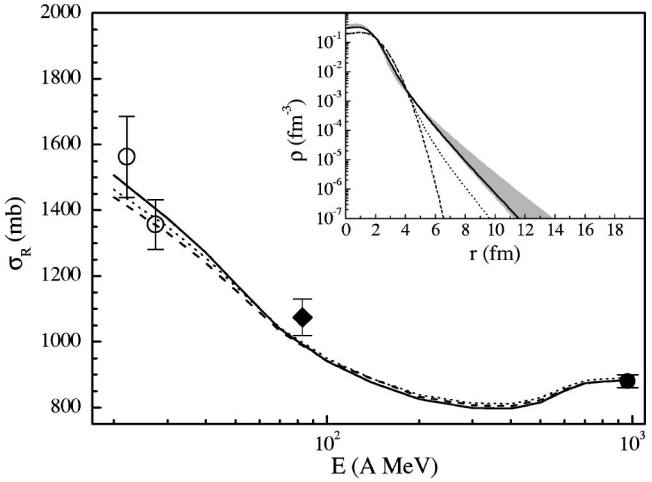

FIG. 6. Energy dependence of the reaction cross section for $^{14}C+^{12}C$. The dashed line is calculated using the finite-range Glauber model with the density of ^{14}C assumed to be HO-type distribution. The dotted and solid lines are calculated using HO core plus $v(p_{1/2})$ neutron and Yukawa tail, respectively. The rhombus is data from the present experimental. Other experimental data using the transmission-type method are shown by solid [20] and open [15,30] circles. Density distributions are shown in the inset. The dashed, dotted, and solid lines are HO, HO plus $v(p_{1/2})$ neutron, and Yukawa tail, respectively. The shaded area refers to the fitted error. For details see text.

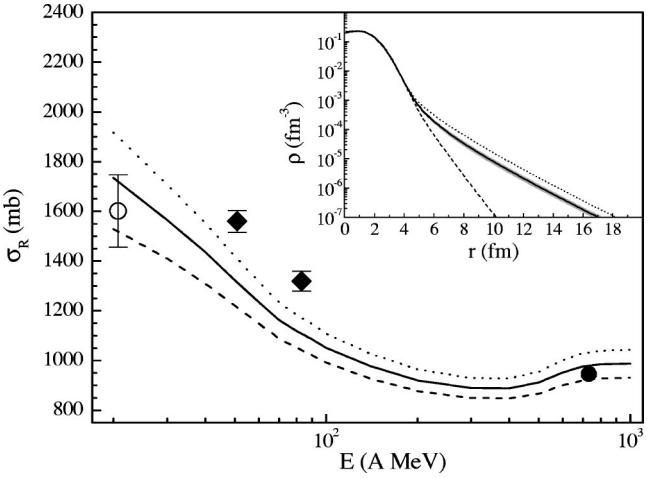

FIG. 7. Energy dependence of the reaction cross section for $^{15}C+^{12}C$. The dotted and dashed lines are calculated using the pure *s* and *d* wave distributions. The solid line is the best fit when admixture between the *s* and *d* waves is considered. The symbols are same as Fig. 6. Density distributions are in the inset. The dotted, dashed, and solid lines are the *s*, *d* wave distribution, and admixture between them. The shaded area refers to the fitted error.

neutron density distribution can explain the momentum distribution of $^{14}C\rightarrow{}^{13}C$ very well. To use similar density distribution in both momentum distribution and reaction cross section analysis, a core (^{13}C) with HO-type distribution plus $v(p_{1/2})$ neutron was assumed for ^{14}C. Then the HO size parameter was adjusted to fit the σ_R data at different energies measured by the transmission-type method. For comparison, a less constraint density distribution was also tried. We assumed HO plus Yukawa tail for the neutron distribution of ^{14}C

$$\rho(r)=\begin{cases}\text{HO-type} & (r<r_c)\\ Y\exp(-\lambda r)/r^2 & (r\geqslant r_c)\end{cases}, \tag{3}$$

where r_c is the crossing point of these two functions and the factor Y is to keep the equality of the two distributions at r_c. The proton density distribution was HO type with the same size parameter. In this method, the size parameter of HO and the slope of the tail were free parameters with r_c determined by the normalization condition $\int\rho(r)d^3r=Z$ where Z is the charge number of the core.

The fitted results from these two methods are plotted in Fig. 6. It was shown that the results calculated from HO plus $v(p_{1/2})$ neutron and Yukawa tail agree with the experimental data a little bit better than that from HO-type distributions. Small difference was also found for HO plus $v(p_{1/2})$ neutron and Yukawa tail distribution. The second method gives a longer tail than the first one but the slope of tail is similar with the *p* wave distribution which can reproduce the momentum distribution of $^{14}C\rightarrow{}^{13}C$. Underestimation for reaction cross section of $^{14}C\rightarrow{}^{12}C$ at low energies may still exist in the finite-range Glauber model.

Regarding the halo structure in ^{15}C, it is interesting to extract information about the density distribution of the valence neutron. Narrow distribution was found in the momentum distribution from the above analysis. It suggests that the valence neutron distribution may have a long tail. But no distinct tail was shown in the analysis of the interaction cross at high energy. In order to extract the effective density distribution for ^{15}C, the energy dependence of σ_R for ^{15}C was also investigated. The density distribution was assumed to be core plus neutron. The fixed HO plus $v(p_{1/2})$ neutron distribution determined from above fitting of ^{14}C data was used for the core. For the valence neutron, admixture between two configurations $0^+\otimes 2s_{1/2}$ and $2^+\otimes 1d_{5/2}$ were considered. The density distributions of ground and excited states were supposed to be same but the excitation energy was added up to the separation energy of the valence neutron. We adjusted the mixing ratio of the *s* and *d* waves to fit the experimental data. The fitted results as well as the pure *s* and *d* waves calculations are compared with the experimental data in Fig. 7. The best fit gives $50\pm8\%$ occupation probability in $v(s_{1/2})$. This value is consistent with the results from the analysis of interaction cross section at relativistic energies [20] since the fitted results reproduce reaction cross section at high energy much better than that at low energies. But it is seen that the fitted results are off the experiment data at low energies.

The effective density distribution of ^{15}C was extracted by another method in which only the reaction cross sections from the present experiment were used. The same HO plus $v(p_{1/2})$ neutron distribution was used for ^{14}C core. Now the HO size parameter was adjusted to reproduce the reaction cross section of ^{14}C at 83*A* MeV. Since the *s* wave still underestimated the experimental cross section, the depth of the

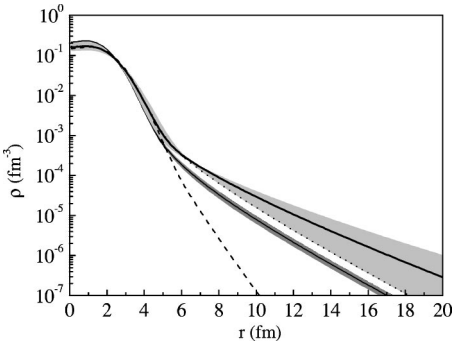

FIG. 8. Density distribution of ^{15}C. Assuming core plus neutron structure, the core density is changed to fit the σ_R data of ^{14}C at 83*A* MeV while the valence neutron distribution is determined by adjusting the depth of the potential arbitrarily to reproduce the σ_R's of ^{15}C at 51*A* MeV and 83*A* MeV from the present measurement. The thick solid line is the best fit result. The dotted and dashed lines show the calculated *s* and *d* wave distributions. The shaded area represents the fitted error. The density distribution shown in Fig. 7 is also plotted here for comparison by the solid line.

Wood-Saxon potential was changed arbitrarily in calculating the wave function of the valence neutron to reproduce the σ_R's of ^{15}C at 51*A* MeV and 83*A* MeV. The best-fitted density is compared with the calculated *s* and *d* wave distributions in Fig. 8. A long tail is necessary to explain the measured reaction cross section of ^{15}C. The extracted tail agrees with the *s* wave distribution much better than the *d* wave. We can conclude that the *s* wave component is dominant in the ground state of ^{15}C from the present analysis. In the figure, the density distribution determined by the previous method was also shown. It should be pointed out that the present method gave a larger core size than previous analysis based on energy dependence of σ_R. But the valence neutron distribution should be reasonable. Since we are interested in valence neutron structure much more than the core, this method can provide us important information about the tail density distribution. The inconsistent conclusions from the two analysis methods may be attributed to the use of a simple reaction model in our analysis as well as inconsistency of the experimental data measured at different energies. Since only σ_R data from the present measurement were used, the conclusion from the present method will be less model dependent than that from the previous one. Thus our analysis of the measured reaction cross section data suggests that the *s* wave component is dominant in the ground state of ^{15}C which is consistent with the conclusion obtained from the momentum distribution analysis.

V. CONCLUSION

In summary, the longitudinal momentum distributions of ^{13,14}C fragments from ^{15}C and ^{13}C fragments from ^{14}C breakup were measured at 83*A* MeV. The reaction cross sections for ^{14,15}C were measured at the same time. The FWHMs for ^{13}C fragments from ^{15}C and ^{14}C breakup are consistent with the Goldhaber model's prediction. Narrow distributions were seen for $^{15}\mathrm{C}\rightarrow{}^{14}\mathrm{C}$ which are consistent with previous measurements. An anomalous enhancement from its neighbors has been observed in the measured reaction cross section of ^{15}C. The experimental results were analyzed in the framework of the Glauber model. The analysis of both the fragment momentum distribution and reaction cross section suggests a dominant s-wave component in the ground state of ^{15}C. It is a strong evidence of halo structure in this nucleus.

ACKNOWLEDGMENTS

The authors gratefully acknowledge all of the staff at the RIKEN accelerator for providing stable beams during the experiment.

[1] I. Tanihata *et al.*, Phys. Rev. Lett. **55**, 2676 (1985).
[2] G. Audi and A. H. Wapstra, Nucl. Phys. **A565**, 66 (1993).
[3] G. Murillo, S. Sen, and S. E. Darben, Nucl. Phys. **A579**, 125 (1994).
[4] J. D. Goss *et al.*, Phys. Rev. C **12**, 1730 (1975).
[5] F. E. Cecil *et al.*, Nucl. Phys. **A255**, 243 (1975).
[6] D. Bazin *et al.*, Phys. Rev. C **57**, 2156 (1998).
[7] V. Maddalena *et al.*, Nucl. Phys. **A682**, 332c (2001).
[8] E. Sauvan *et al.*, Phys. Lett. B **491**, 1 (2000); nucl-ex/0307019, Phys. Rev. C (to be published).
[9] A. S. Goldhaber, Phys. Lett. **53B**, 306 (1974).
[10] U. Datta Pramanik *et al.*, Phys. Lett. B **551**, 63 (2003).
[11] A. Ozawa *et al.*, Nucl. Phys. **A693**, 32 (2001).
[12] W. Mittig *et al.*, Phys. Rev. Lett. **59**, 1889 (1987).
[13] M. G. Saint-Laurent *et al.*, Z. Phys. A **332**, 457 (1989).
[14] A. C. C. Villari *et al.*, Phys. Lett. B **268**, 345 (1991).
[15] D. Q. Fang *et al.*, Phys. Rev. C **61**, 064311 (1999).
[16] L. Chulkov *et al.*, Nucl. Phys. **A674**, 330 (2000).
[17] T. Zheng *et al.*, Nucl. Phys. **A709**, 103 (2002).
[18] T. Yamaguchi *et al.*, Nucl. Phys. **A724**, 3 (2003).
[19] V. Maddalena *et al.*, Phys. Rev. C **63**, 024613 (2001).
[20] A. Ozawa *et al.*, Nucl. Phys. **A691**, 599 (2001).
[21] R. Kanugo *et al.*, Phys. Rev. Lett. **88**, 142502 (2002).
[22] N. Iwasa *et al.*, Nucl. Instrum. Methods Phys. Res. B **126**, 284 (1997).
[23] J. A. Tostevin, Nucl. Phys. **A682**, 320c (2001).
[24] P. G. Hansen and B. M. Sherrill, Nucl. Phys. **A693**, 133 (2001).
[25] Y. L. Parfenova *et al.*, Phys. Rev. C **62**, 044602 (2000).
[26] Y. Ogawa, Y. Suzuki, and K. Yabana, Nucl. Phys. **A571**, 784 (1994).
[27] J. A. Tostevin, J. Phys. G **25**, 735 (1999).
[28] A. Ozawa *et al.*, Nucl. Phys. **A608**, 63 (1996).
[29] M. Fukuda *et al.*, Nucl. Phys. **A656**, 209 (1999).
[30] H. Y. Zhang *et al.*, Nucl. Phys. **A707**, 303 (2002).